Malaysian Journal of Mathematical Sciences 20(2): 511–535 (2026)
https://doi.org/10.47836/mjms.20.2.04

Malaysian Journal of Mathematical Sciences

Journal homepage: https://mjms.upm.edu.my

Mathematical Modelling of Blood Flow Narrowing in Left Coronary Artery Causing Cardiovascular Disease Using Finite Volume Method

Fatahillah, A.* [1], Hamdan, M. S. F. [1], Prihandini, R. M. [1], and Roslan, R. [2]

[1]*Department of Mathematics Education, University of Jember, Jember, Indonesia*
[2]*Department of Mathematics and Statistics, Faculty of Applied Sciences and Technology, Universiti Tun Hussein Onn Malaysia, Pagoh Campus, 84600 Muar, Johor, Malaysia*

E-mail: arif.fkip@unej.ac.id
**Corresponding author*

Received: 2 July 2025
Accepted: 31 October 2025

Abstract

This study investigates the behavior of blood flow in the Left Coronary Artery (LCA) experiencing symmetrical narrowing, focusing on three stenosis geometries: triangular, trapezoidal, and overlapping (W-shape). It aims to develop a mathematical model of post-stenotic flow, assess the effectiveness of the Finite Volume Method (FVM), and analyze how stenosis shape and severity affect velocity and pressure. The governing equations of fluid motion are solved using FVM for spatial discretization and the SIMPLE algorithm to compute flow variables. Results show that FVM accurately simulates blood dynamics in narrowed arterial regions. Notably, when stenosis exceeds 50%, flow velocity increases significantly, reaching a peak at 75% narrowing. This condition also corresponds to a sharp pressure drop, especially in the trapezoidal model, indicating a higher potential for vascular damage and plaque accumulation. These changes in hemodynamic behavior highlight the critical role of stenosis geometry in altering blood flow. Therefore, understanding the influence of narrowing shape and severity is essential for clinical assessment and early diagnosis of coronary artery disease.

Keywords: blood flow; triangular; trapezoidal; overlapping (W-shape); SIMPLE algorithm.

1 Introduction

Atherosclerosis is one of the most common and impactful cardiovascular diseases worldwide. Over the past several decades, numerous studies have been conducted to understand its causes and developmental mechanisms. Atherosclerosis arises due to progressive disturbances in the arterial wall that cause irregularities in blood flow. This condition promotes the formation of plaques that gradually narrow the blood vessels throughout the cardiac cycle [21, 18]. Over time, the blood vessels become increasingly narrow and stiff, thereby obstructing the blood supply to vital organs. If this condition persists, the narrowing can trigger serious complications such as heart attacks or strokes [14, 3]. In Indonesia, according to World Health Organization (WHO) data, cardiovascular diseases are the leading cause of death from non-communicable diseases (35%), followed by diabetes (6%) [28].

One of the most dangerous forms of atherosclerosis is coronary artery disease (CAD), which occurs when plaques accumulate on the inner walls of the coronary arteries. These plaques are composed of a combination of fats, cholesterol, calcium, and other substances that build up in areas experiencing damage or inflammation. As the accumulation increases, the arterial lumen narrows and impedes oxygen-rich blood flow to the heart muscle. When oxygen supply is disrupted, patients may experience symptoms such as chest pain (angina pectoris). In more severe cases, plaque rupture can trigger the formation of blood clots that can completely block the artery, causing a heart attack (myocardial infarction) [15, 6].

A study titled "Numerical computation of blood hemodynamic through constricted human left coronary artery: Pulsatile simulations" utilizes the non-Newtonian Carreau viscosity model to describe the hemodynamic behavior of blood at various levels of blockage throughout the cardiac cycle. This model provides a deeper understanding of the effects of narrowing on blood flow [21]. Inspired by this approach, the present research develops a mathematical model of blood flow in a stenosed LCA, as this condition is a primary contributor to cardiovascular disease. In addition to studying the shape of the arterial narrowing, this research considers stenosis levels of 25%, 50% and 75%, as well as differences in the stenosis position along the artery to assess the impact of narrowing location on blood flow characteristics. The choice of stenosis levels at 25%, 50% and 75% in this study is based on the aim to evaluate the effects of different degrees of narrowing on blood flow hemodynamics. These levels reflect the severity commonly encountered in coronary artery disease, ranging from mild to severe stenosis [11].

The finite volume method was chosen because it can handle complex geometries such as the blood vessel structure shown in Figure 1, and it allows for accurate discretization through the formation of structured grids. This method is highly effective for analyzing unstructured shapes [19, 33]. In its implementation, the SIMPLE algorithm (Semi-Implicit Method for Pressure-Linked Equations) is used to resolve the coupling between pressure and velocity based on the conservation equations of mass and momentum [16, 24]. Numerical methods like the SIMPLE algorithm have been proven accurate and efficient in simulating blood flow through arteries with stenosis. Its reliability, validated through comparisons with ANSYS fluent, makes this method suitable for analyzing blood flow in the stenosed LCA, a key factor in cardiovascular disease [7, 2]. To support the computational process, MATLAB is used for simulation and visualization of numerical results, while ANSYS fluent is employed for comprehensive fluid-structure interaction analysis on the arterial model [8, 29]. Under the title numerical analysis of blood flow constriction in the LCA causing cardiovascular disease using the finite volume method, this study aims to develop simulation models of three types of constriction shapes: triangular, trapezoidal, and overlapping (W-shape), with variations in plaque thickness and different stenosis locations. The primary goal is to evaluate the impact of stenosis geometry and position on velocity, pressure, and wall shear

stress, as well as to contribute to the development of more effective diagnostic and therapeutic methods for cardiovascular diseases.

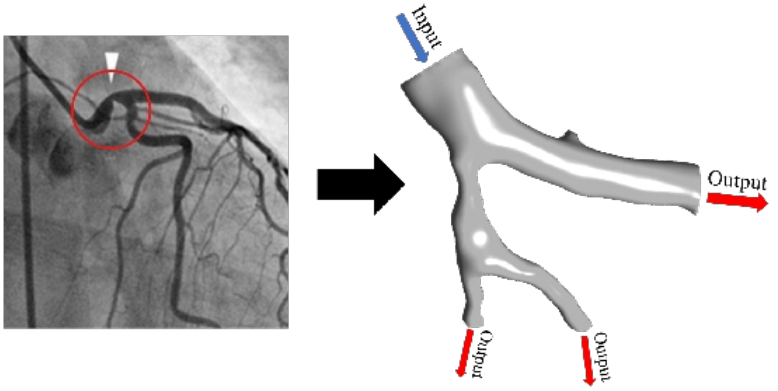

Figure 1: The image on the left shows the constricted area of the LCA, marked with a red circle, while the right side depicts the artery model representation with indicated inlet and outlet flow directions. This setup is used to analyze the blood flow dynamics in the presence of stenosis [22].

2 Materials and Methods

2.1 Mathematical formulation

This research commences with the formulation of a mathematical framework to investigate hemodynamics and their effect on cardiac perfusion within the LCA.The study employs three distinct symmetrical stenosis geometries: triangular, trapezoidal, and overlapping (W-Shape), as illustrated in Figure 2. These three stenosis geometries were specifically chosen to investigate how different characteristics of the peak constriction affect hemodynamics. The Triangular shape models a sharp, pointed peak, the Trapezoidal shape represents a peak with a constant, flat width, while the Overlapping (W-Shape) simulates a more complex, wavy peak profile. By systematically analyzing these distinct peak morphologies, this study aims to determine how the specific shape of a blockage whether sharp, flat, or irregular directly influences critical flow parameters such as blood velocity, pressure drop, and wall shear stress. These three shapes are used to represent variations in stenosis geometry within blood vessels that influence velocity and pressure in blood flow. Many previous studies have adopted these shapes, facilitating comparison of research results using similar geometries.

The equations presented below form the foundation of this study's approach to modeling blood flow dynamics. The Conservation of Mass equation ensures that mass is conserved within the flow, while the Conservation of Momentum equation governs the motion of the blood through the arteries. These equations are crucial for understanding how the fluid behaves under different stenosis conditions [30, 31].

Mass equation [27, 31],

$$\nabla \cdot \vec{V} = 0. \tag{1}$$

Momentum equation [31],

$$\rho\left(\frac{\partial\vec{V}}{\partial t}+\left(\vec{V}\cdot\nabla\right)\vec{V}\right)=-\nabla p+\mu\nabla^2\vec{V}, \tag{2}$$

with

$$\begin{aligned}\vec{V}&=\text{Fluid velocity vector (m/s)},\\ \rho&=\text{Fluid density (kg/m}^3),\\ p&=\text{Fluid pressure (Pa)},\\ \mu&=\text{Dynamic viscosity of the fluid (Pa.s)}.\end{aligned}$$

The boundary conditions for the stenosis radius in arteries with triangular, trapezoidal, and overlapping (W-shape) stenosis are as follows [20, 35].

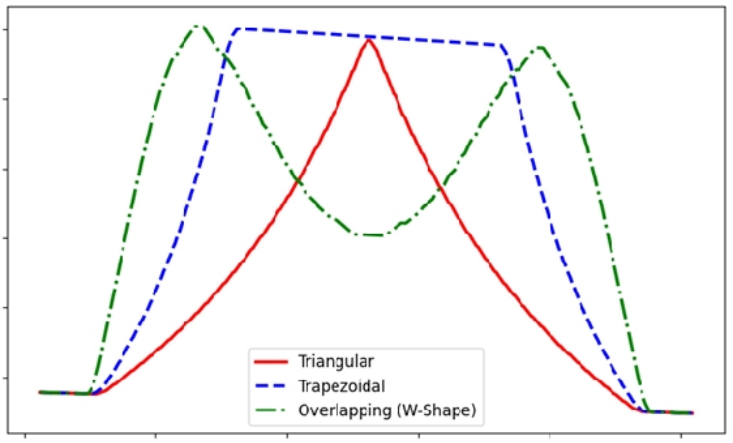

Figure 2: The stenotic artery is represented through three distinct geometric profiles: Triangular, trapezoidal, and W shaped overlapping forms.

Triangular shaped equation [20],

$$R_1\left(\bar{z}\right)=\begin{cases}\bar{R}_0-\dfrac{2\bar{\delta}_1}{\bar{R}_0}\left(\bar{z}-\bar{d}_1\right), & \bar{d}_1\le\bar{z}\le\bar{d}_1+\dfrac{\bar{L}_{0_1}}{2},\\ \bar{R}_0-\dfrac{2\bar{\delta}_1}{\bar{R}_0}\left(\bar{L}_{0_1}+\bar{z}-\bar{d}_1\right), & \bar{d}_1+\dfrac{\bar{L}_{0_1}}{2}\le\bar{z}\le\bar{d}_1+\bar{L}_{0_1},\\ \bar{R}_0, & \text{otherwise.}\end{cases} \tag{3}$$

A schematic illustration of the triangular shaped arterial constriction model is shown on the left, followed by the mathematical equations describing the variation of the artery radius along the stenosis position in the image on the right of Figure 3.

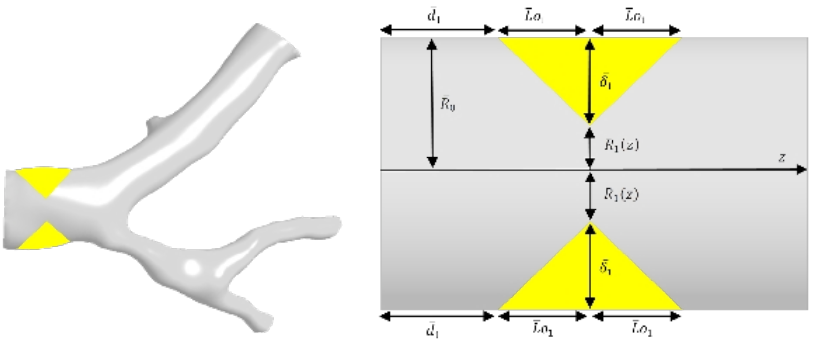

Figure 3: Schematic representation of the triangular model.

Trapezoidal shaped equation [20],

$$R_2(\bar{z}) = \begin{cases} \bar{R}_0 - \dfrac{4\bar{\delta}_2}{\bar{R}_0}\left(\bar{z} - \bar{d}_2\right), & \bar{d}_2 \le \bar{z} \le \bar{d}_2 + \dfrac{\bar{L}_{0_2}}{4}, \\ \bar{R}_0 - \dfrac{\bar{\delta}_2}{\bar{R}_0}\bar{L}_{0_2}\bar{d}_2 + \dfrac{\bar{L}_{0_2}}{4}, & \bar{d}_2 + \dfrac{\bar{L}_{0_2}}{4} \le \bar{z} \le \bar{d}_2 + \dfrac{3\bar{L}_{0_2}}{4}, \\ \bar{R}_0 - \dfrac{2\bar{\delta}_2}{\bar{R}_0}\left[\bar{L}_{0_2} - 2\left(\bar{z} - \bar{d}_2 - \dfrac{\bar{L}_{0_2}}{2}\right)\right], & \bar{d}_2 + \dfrac{3\bar{L}_{0_2}}{4} \le \bar{z} \le \bar{d}_2 + \bar{L}_{0_2}, \\ \bar{R}_0, & \text{otherwise.} \end{cases} \tag{4}$$

The schematic representation of the arterial constriction model with a trapezoidal shape is shown on the left, along with the mathematical equations describing the variation of the artery radius according to the stenosis position in the image on the right of Figure 4.

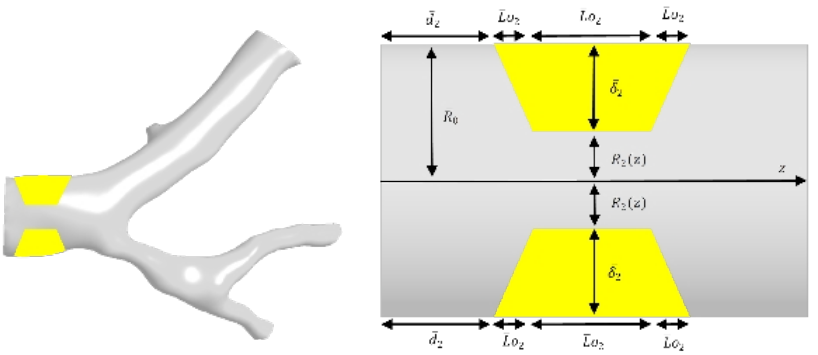

Figure 4: Schematic representation of the trapezoidal model.

Overlapping (W shaped) equation [34, 35],

$$R_3(\bar{z}) = \begin{cases} \bar{R}_0 - \dfrac{3\bar{\delta}_3}{2\bar{L}_{0_3}}\left(11\left(\bar{z}-\bar{d}_3\right)\bar{L}_{0_3}^3 - 47\left(\bar{z}-\bar{d}_3\right)^2\bar{L}_{0_3}^2\right) \\ \quad +72\left(\bar{z}-\bar{d}_3\right)^3\bar{L}_{0_3} - 36\left(\bar{z}-\bar{d}_3\right)^4, & \bar{d}_3 \le \bar{z} \le \bar{d}_3 + \dfrac{\bar{L}_{0_3}}{4}, \\ \bar{R}_0, & \text{otherwise.} \end{cases} \tag{5}$$

A schematic illustration of the overlapping (W-shape) arterial constriction model is shown on the left, followed by the mathematical equations describing the variation of the artery radius along the stenosis position in the image on the right of Figure 5.

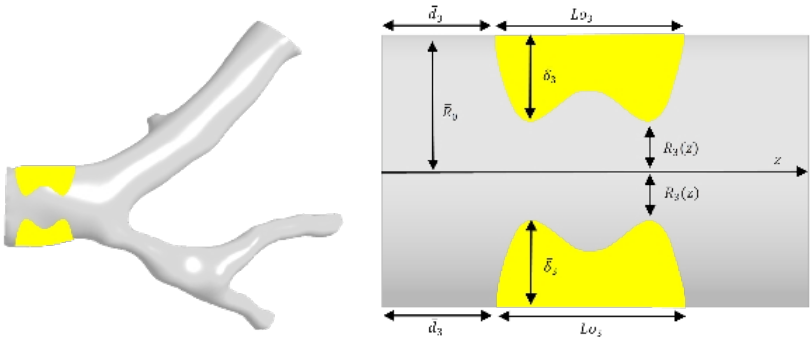

Figure 5: Schematic representation of the overlapping (W-shape) model.

with

$\bar{R}_0 =$ Radius of normal blood vessel,
$R_1(\bar{z}) =$ Radius of stenotic blood vessel for triangular shape,
$R_2(\bar{z}) =$ Radius of stenotic blood vessel for trapezoidal shape,
$R_3(\bar{z}) =$ Radius of stenotic blood vessel for overlapping (W-shape),
$\bar{\delta}_1 =$ Maximum stenosis depth for triangular shape,
$\bar{\delta}_2 =$ Maximum stenosis depth for trapezoidal shape,
$\bar{\delta}_3 =$ Maximum stenosis depth for overlapping (W-Shape),
$\bar{L}_{0_1} =$ Total stenosis length for triangular shape,
$\bar{L}_{0_2} =$ Total stenosis length for trapezoidal shape,
$\bar{L}_{0_3} =$ Total stenosis length for overlapping (W-shape),
$\bar{d}_1 =$ Stenosis location for triangular shape,
$\bar{d}_2 =$ Stenosis location for trapezoidal shape,
$\bar{d}_3 =$ Stenosis location for overlapping (W-shape),
$\bar{z} =$ Blood flow location along the $z-$axis in the vessel system,
$\bar{L} =$ Total artery length,
$m =$ Parametric constant used in the model.

2.2 Flow assumptions and boundary conditions

To accurately model the hemodynamics within the LCA, the flow regime and boundary conditions were established based on relevant physiological principles and standard practices in computational fluid dynamics. The blood flow within the LCA was modeled as laminar. This assumption is justified by a calculated Reynolds number (Re) of 216, as detailed in (6), which is well below the critical threshold (2000) for the onset of turbulence [13]. Therefore, the representation of an orderly flow is considered valid. At the inlet, a fully developed parabolic velocity profile was applied, in accordance with (7). This profile represents a stable Poiseuille flow from the aorta and accurately describes the velocity distribution, with a maximum value at the vessel's centerline and zero at the arterial wall. Subsequently, a zero-pressure gradient condition was imposed on all three outlets. This standard condition simulates the flow proceeding into the downstream vascular network without introducing significant pressure changes that could artificially affect the simulation results, there by ensuring that the observed hemodynamic alterations are purely a function of the geometry and fluid viscosity.

Table 1 shows the parameter values that influence the blood flow rate in the model, including values for blood density, blood viscosity [32], high blood pressure [5], Left Main Stem (LMS) diameter [23], and initial velocity [17].

Table 1: Numerical values of parameters influencing blood flow rate.

Parameters	**Value**
Blood density	1050 kg/m^3
Blood viscosity	0.0035 Pa.s
High blood pressure	130/80 mmHg
Left Main Stem (LMS) diameter	3.0 mm
Initial velocity	0.24 m/s

Once the relevant parameters influencing blood flow in the LCA are established, the Reynolds number is computed using the following expression to classify the flow type under stenotic [13],

$$Re = \frac{\rho U D}{\mu}. \tag{6}$$

The study provides the inlet velocity value as shown in the following equation [25, 10],

$$u = 2U_0 \left(1 - \left(\frac{r}{R(\bar{z})}\right)^2\right), \qquad \text{at the inlet } (x = 0). \tag{7}$$

Pousielle's law states that fluid flow through a cylindrical pipe with length L and transverse radius r can be determined by the formula [4],

$$Q = \frac{\pi \Delta P r^4}{8\eta L}, \tag{8}$$

where ΔP is the pressure gradient, η is the viscosity of the fluid, L is the length of the tube, Q is the flow, and r is the radius of the tube.

2.3 Methodology

This research utilizes MATLAB in conjunction with the SIMPLE algorithm to solve partial differential equations relevant to fluid dynamics. The SIMPLE algorithm, widely adopted in Computational Fluid Dynamics (CFD), serves as a robust approach for resolving the primary governing equations of fluid motion. To solve the governing Navier-Stokes equations, the numerical implementation utilizes computational methods. Specifically, temporal integration is handled by the Euler method, while spatial derivatives are approximated using finite difference schemes [31]:

1. Set initial guesses for p^*, u^*, v^*, and φ^*.
2. Equations (9) and (10) show the finite volume discretization of the momentum equations in the Finite Volume Method (FVM), where fluid flow through cell faces is calculated based on pressure gradients and neighboring velocity values. These equations are used in the velocity prediction step of the SIMPLE algorithm;

$$a_{i,j}u^*_{i,j} = \sum a_{n,b}u_{n,b} + \left(p^*_{i-1,j} - p^*_{i,j}\right)A_{i,j} + b_{i,j}, \tag{9}$$

$$a_{i,j}v^*_{i,j} = \sum a_{n,b}v_{n,b} + \left(p^*_{i,j-1} - p^*_{i,j}\right)A_{i,j} + b_{i,j}. \tag{10}$$

3. Solve the pressure correction equation,

$$a_{i,j}p'_{i,j} = a_{i+1,j}p'_{i+1,j} + a_{i-1,j}p'_{i-1,j} + a_{i,j+1}p'_{i,j+1} + a_{i,j-1}p'_{i,j-1} + b_{i,j}. \tag{11}$$

4. Determine the corrected pressure and velocities,

$$u_{i+1,j} = u^*_{i+1,j} + d_{i+1,j}\left(p'_{i,j} - p'_{i+1,j}\right), \tag{12}$$

$$v_{i,j+1} = v^*_{i,j+1} + d_{i,j+1}\left(p'_{i,j} - p'_{i,j+1}\right), \tag{13}$$

where

$$d_{i+1,j} = \frac{A_{i+1,j}}{A_{i,j}} \quad \text{and} \quad d_{i,j} = \frac{A_{i,j}}{A_{i+1,j}}. \tag{14}$$

5. Solve all discretized transport equations,

$$a_{i,j}\varphi_{i,j} = a_{i+1,j}\varphi_{i+1,j} + a_{i-1,j}\varphi_{i-1,j} + a_{i,j+1}\varphi_{i,j+1} + a_{i,j-1}\varphi_{i,j-1}. \tag{15}$$

6. Verify whether the numerical solution has reached convergence; if convergence is not met, iterate through Steps 1 to 4 until stability is attained.

with

$a_{i,j}$ = Discretization coefficient for velocity at point (i,j),
$u^*_{i,j}$ = Predicted velocity component u at point (i,j),
$v^*_{i,j}$ = Predicted velocity component v at point (i,j),
$p^*_{i,j}$ = Predicted pressure at point (i,j),
$A_{i,j}$ = Control volume area at point (i,j),
$b_{i,j}$ = Source or additional coefficient at point (i,j),
$d_{i,j}$ = Correction factor at point (i,j),
$\varphi_{i,j}$ = Transport variable at point (i,j).

MATLAB is employed in this research to implement and validate the SIMPLE algorithm, with the objective of maintaining the stability and reliability of the numerical outcomes [21]. After the validation process, the simulation outcomes are compared with those generated by ANSYS Fluent to evaluate the reliability of the developed computational model. Despite MATLAB employing a more straightforward numerical framework, the results exhibit strong agreement with those obtained via ANSYS Fluent, a software known for its advanced capabilities in Computational Fluid Dynamics (CFD). The analysis emphasizes key hemodynamic parameters, including pressure profiles, velocity fields, and fluid behavior in the vicinity of the stenotic region. This validation step is essential to confirm that the MATLAB-based SIMPLE algorithm produces results with sufficient accuracy before being applied to more complex simulation cases [9].

3 Results and Discussion

To validate the MATLAB simulation, its results were benchmarked against outputs from ANSYS Fluent. This process aimed to evaluate the computational model's accuracy and ascertain the SIMPLE algorithm's effectiveness in capturing blood flow characteristics for three distinct stenosis geometries (triangular, trapezoidal, and overlapping/W-shape). The analysis centered on the velocity and pressure distributions along the narrowed vessels.

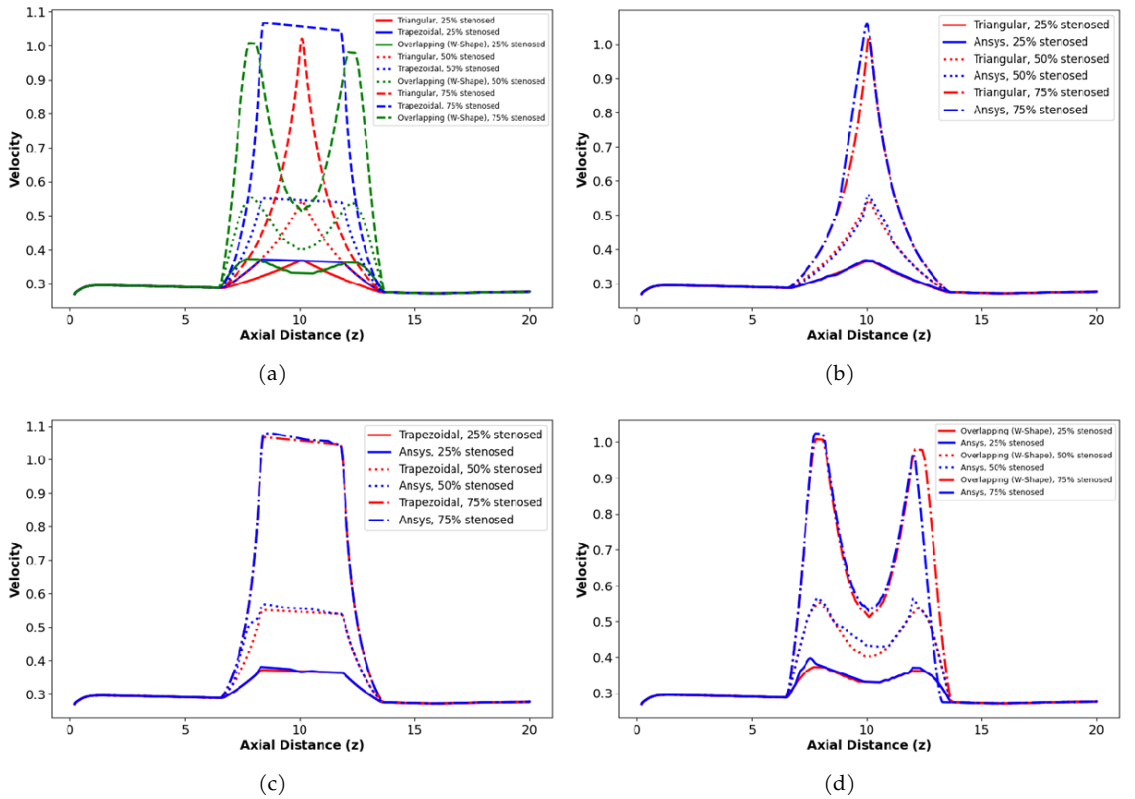

Figure 6: Comparative analysis of axial blood flow velocity: (a) All geometric models, (b) ANSYS simulation of triangular stenosis, (c) ANSYS simulation of trapezoidal stenosis, (d) ANSYS simulation of overlapping W shaped stenosis.

As depicted in Figure 6, the velocity profiles generated by both MATLAB and ANSYS Fluent show strong agreement, with maximum velocities consistently observed at the stenotic centeran effect most pronounced in the trapezoidal geometry. Nevertheless, ANSYS Fluent reveals a sharper velocity gradient, most notably under 75% narrowing, which may be attributed to finer mesh resolution and enhanced turbulence modeling. The plotted velocity distributions distinguish between physiological and pathological flow regimes. Although blood flow is generally stable at stenosis levels ranging from 25% to 50%, a significant increase in velocity is observed at 75%, exceeding the normal limit of 0.5 m/s. This condition indicates a shift toward unstable hemodynamics, which may pose serious clinical implications. The 75% constriction is especially severe, characterized by the highest peak in flow velocity and substantial disturbance in flow patterns. This significant increase in velocity at the stenosis throat is physically governed by the principle of conservation of mass (the continuity equation). As the arterial cross-sectional area narrows due to plaque, the fluid (blood) must accelerate to maintain a constant volumetric flow rate. Clinically, this high-velocity jet not only elevates the shear forces on the arterial wall but can also lead to unstable or turbulent flow in the post-stenotic region, potentially damaging endothelial cells and accelerating disease progression. Of all geometries examined, the trapezoidal model produced the highest velocity values, suggesting a greater likelihood of turbulent flow and elevated wall shear stress factors associated with severe hemodynamic disturbances.

Figure 7 show the comparison of flow velocity profiles between simulation results (red, dashed) and data from other research (blue, solid) for three different cases. Case 7(a) shows a triangular profile, 7(b) a trapezoidal profile and 7(c) a overlapping (W-shaped) profile. The simulation results consistently match the reference data, confirming the model's validity.

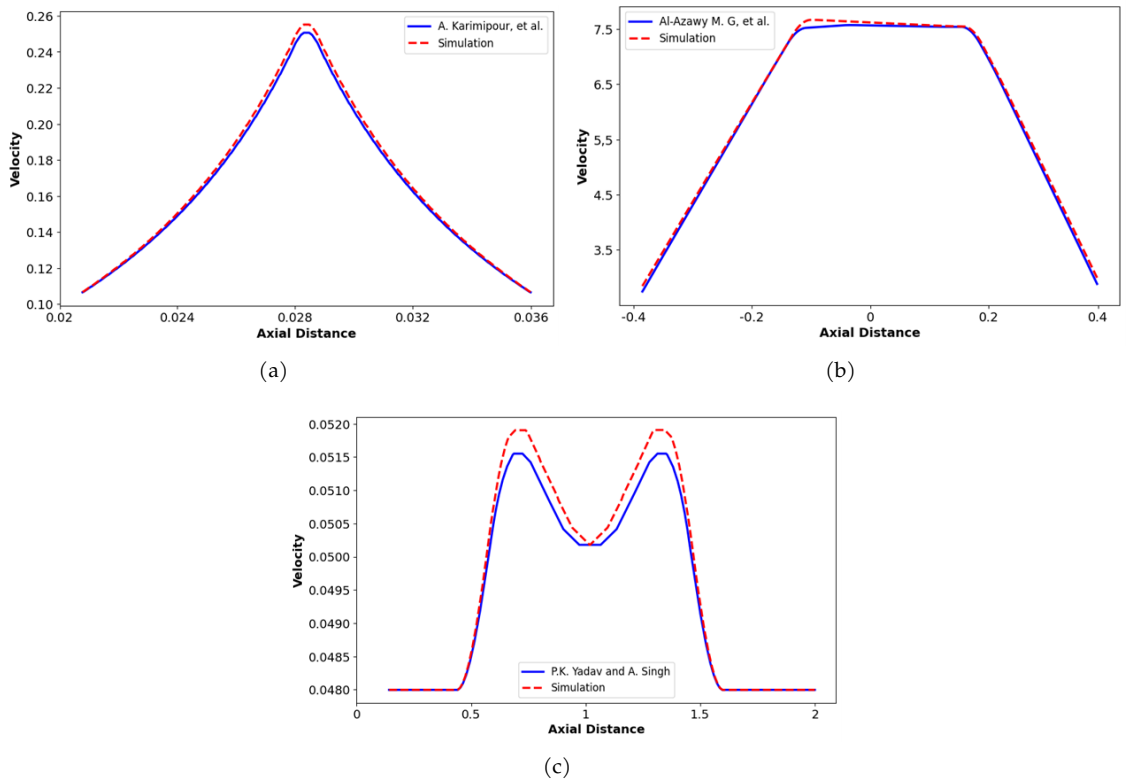

Figure 7: Comparison of Simulation Results with Experimental Data. This graph displays the simulated flow velocity for various conditions. The model's reliability is confirmed by its excellent agreement with the experimental data [12, 1, 34].

The comparative pressure analysis depicted in Figure 8 reveals that as the degree of stenosis intensifies, the resulting pressure drop becomes more substantial, particularly at the site of maximum narrowing. The subfigures 8(b)−8(d) illustrate that the pressure trends obtained from the MATLAB simulations are generally in agreement with those from ANSYS Fluent. However, at a stenosis severity of 75%, ANSYS Fluent demonstrates a steeper decline in pressure, especially near the constricted segment. This discrepancy may stem from differences in numerical schemes or parameter settings between the two platforms. Despite slight variations, both simulation tools exhibit a consistent pattern: greater narrowing correlates with increased pressure loss around the stenotic region.

As shown in Figure 8, the most significant pressure reduction occurs at 75% stenosis, indicating critical hemodynamic consequences such as elevated turbulence, heightened shear stress, and an increased likelihood of vessel wall collapse. The drastic pressure drop at the point of maximum constriction is a direct manifestation of the Bernoulli principle. This principle states that for an ideal fluid flow, an increase in velocity is accompanied by a decrease in pressure. The kinetic energy of the blood increases (due to high velocity), which must be balanced by a decrease in potential energy in the form of pressure. This sharp pressure drop creates an adverse pressure gradient in the distal region of the stenosis, which can lead to flow separation. These separation zones are often characterized by low and recirculating velocities, providing an ideal environment for platelet aggregation and further plaque deposition. Moreover, transitioning from 50% to 75% narrowing leads to an even more pronounced pressure gradient, particularly in the Trapezoidal and Overlapping models, reflecting a shift from normal flow to disturbed conditions.

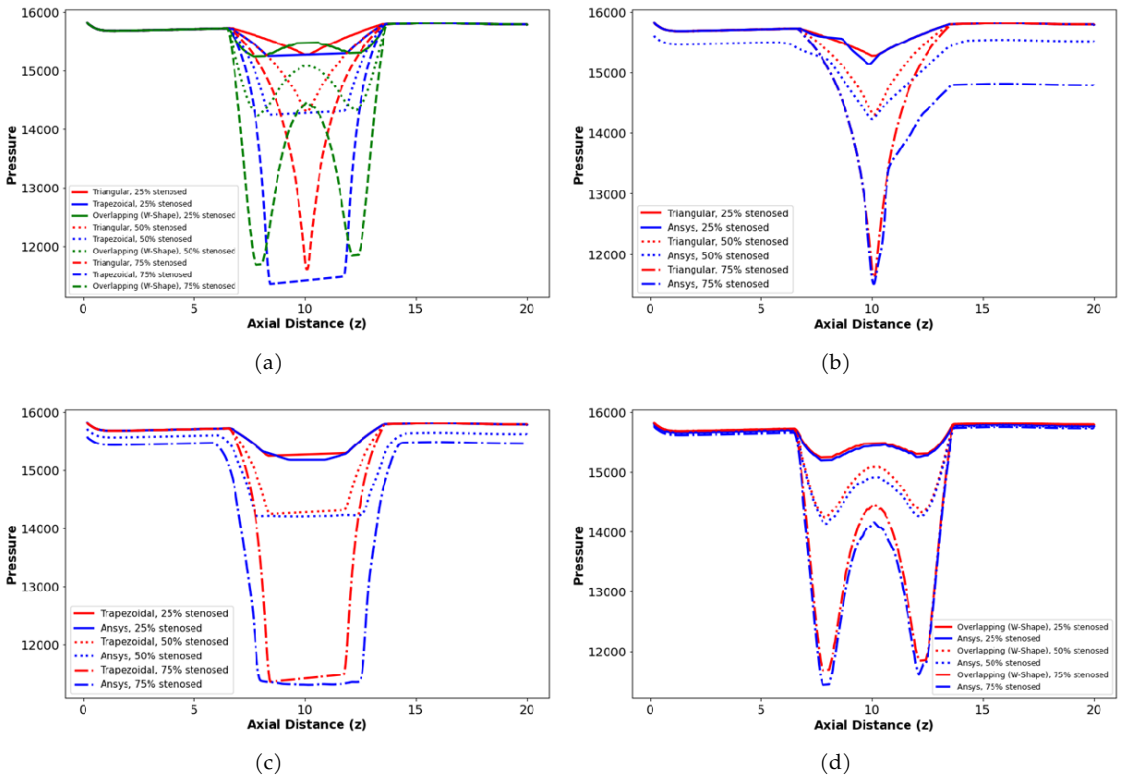

Figure 8: Comparative analysis of axial blood flow pressure: (a) All geometric models, (b) ANSYS simulation of triangular stenosis, (c) ANSYS simulation of trapezoidal stenosis, (d) ANSYS simulation of overlapping W shaped stenosis.

The numerical solution was obtained using MATLAB, based on the Finite Volume Method (FVM), where governing equations are solved on a discretized mesh. For the triangular stenosis model, Figure 8(b) illustrates the effect of stenosis severity on the velocity profile. As the available flow area shrinks with stenosis increasing from 25% to 75%, local velocity varies substantially. Simulation results confirm this, showing a velocity increase from 0.37 m/s (25% stenosis) to 1.06 m/s (75% stenosis) and highlighting the strong correlation between constriction severity and flow disturbance.

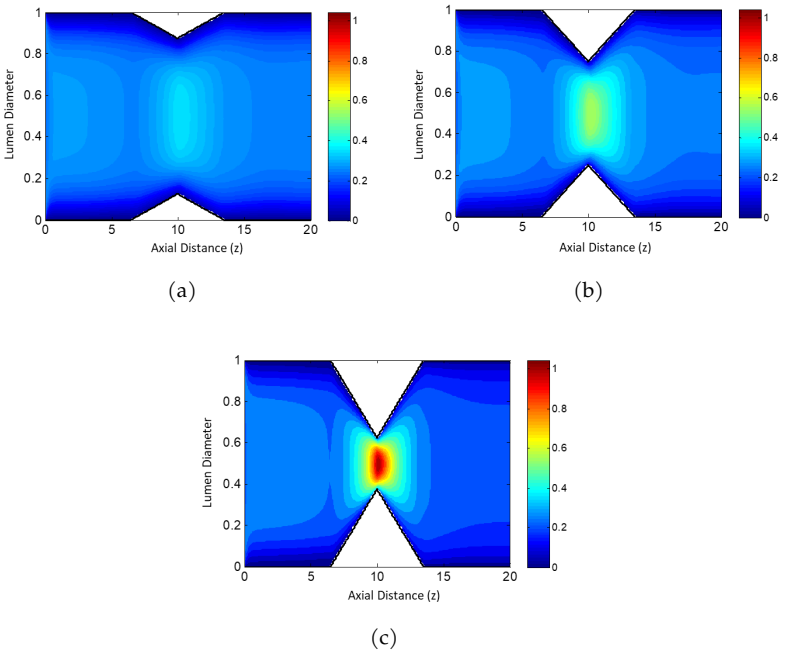

Figure 9: Flow velocity contours corresponding to various stenosis severities in symmetric Triangular shaped geometry: (a) 25% stenosis, (b) 50% stenosis, (c) 75% stenosis.

In the triangular stenosis, the shape changes gradually, resembling an increasingly larger triangle. From Figures 9(a)–9(c), show that as the stenosis level increases, the flow velocity in the constricted area becomes higher. For example, in the 25% stenosis shown in Figure 9(a), the velocity increase is still relatively low, marked by a dominant yellow-green area. Conversely, at 75% stenosis in Figure 9(c), a much more drastic velocity increase (1.056 m/s) occurs, seen from the more pronounced orange-red area at the stenosis center. This illustrates the principle of continuity, where the fluid accelerates to pass through the smaller cross-sectional area. Moreover, the velocity surge is more significant at higher stenosis levels, potentially increasing the risk of vessel wall rupture.

In the trapezoidal stenosis, the change from the initial diameter to the smallest diameter follows the trapezoidal geometry pattern, resulting in different changes compared to the triangular shape, especially regarding the reduction and increase of diameter. In Figures 10(a) and 10(b), which show 25% and 50% stenosis respectively, the flow pattern remains similar with maximum velocity still concentrated in the narrowest area. However, as illustrated in Figure 10(c), when the degree of stenosis reaches 75%, there is a substantial increase in flow velocity, peaking at approximately 1.06755 m/s within the narrowed region. This acceleration is visually indicated by the pronounced red coloration at the core of the constriction.

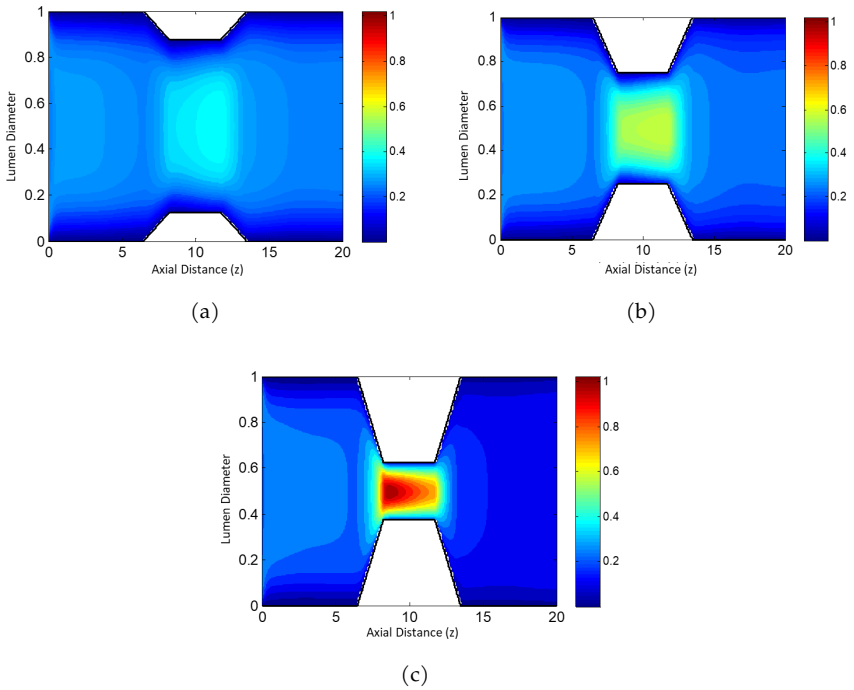

Figure 10: Flow velocity contours corresponding to various stenosis severities in symmetric Trapezoidal shaped geometry: (a) 25% stenosis, (b) 50% stenosis, (c) 75% stenosis.

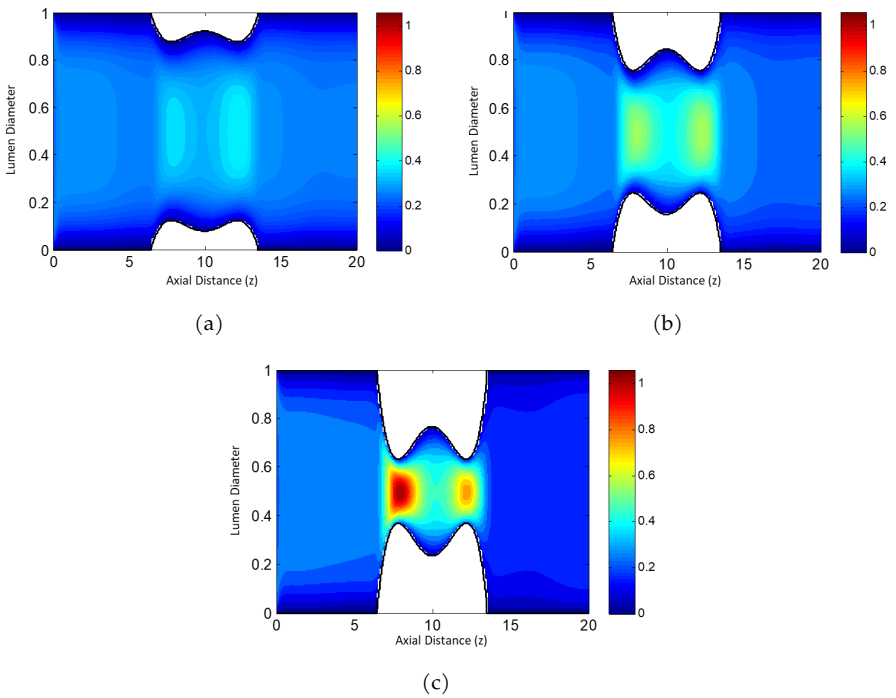

Figure 11: Flow velocity contours corresponding to various stenosis severities in symmetric Overlapping (W-shape) geometry: (a) 25% stenosis, (b) 50% stenosis, (c) 75% stenosis.

The w-shape stenosis tends to have a gentler peak compared to triangular and trapezoidal shapes. In Figures 11(a)−11(c), the velocity increase is clearly visible as the stenosis percentage increases. The pattern is similar to the previous stenosis types, where the larger the stenosis, the higher the peak velocity in the narrowest area. However, compared to triangular and trapezoidal shapes, the velocity contour at 50% stenosis appears more uniform, indicating that the flow may be more distributed before experiencing a sharp increase $(1.008\ \text{m/s})$ at 75% stenosis.

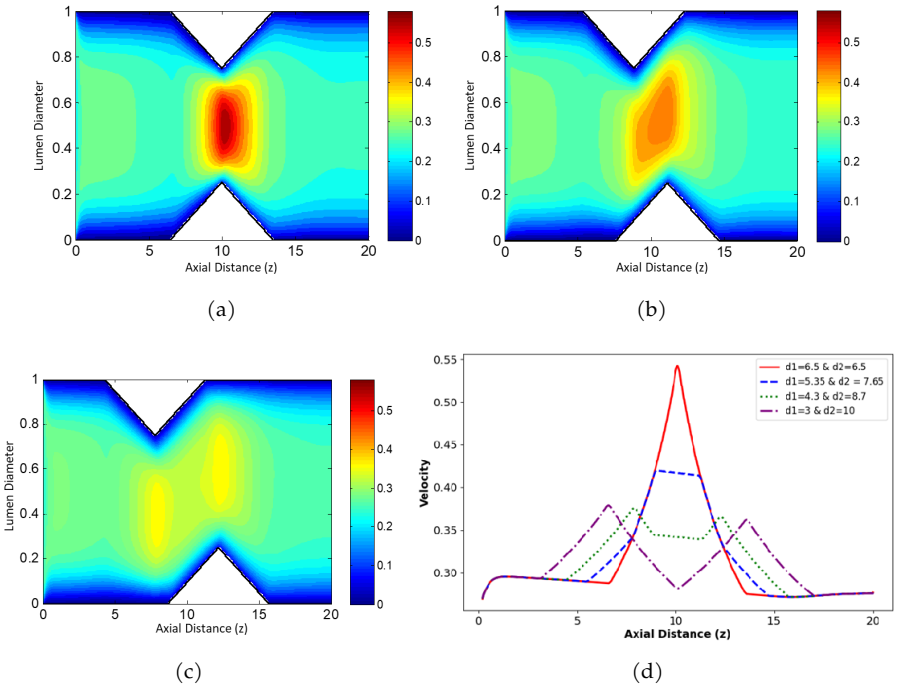

Figure 12: Flow velocity contours for different stenosis locations within a symmetric Triangular geometry.

In Figure 12(a), the high-velocity region marked by yellow to red colors accumulates around the stenosis peak, causing the fluid to be immediately pushed to narrow. After passing the constricted zone, the flow expands again, causing the velocity to decrease, as seen from the dominance of yellow-green colors. In Figures 12(b)−12(b), the velocity increase is more dominant in the shifted area, following the stenosis location. Additionally, flow in the stenosis region tends to have relatively lower velocity. The farther the stenosis position shifts, the longer the upstream region where the flow is undisturbed before accelerating into the stenosis, which can affect the velocity pattern of blood flow in the LCA.

In Figure 13(a), flow accelerates around the stenosis area, resulting in a more visible red zone (indicating high velocity) in that region. After passing the narrowed part, flow velocity starts to decrease, shown by yellow colors. Figures 13(b)−13(d) show a more pronounced velocity increase in the shifted stenosis area according to its position. Within the stenosis zone, flow tends to have relatively lower velocity. Overall, the farther the stenosis position shifts, the longer the area where the fluid prepares before acceleration at the stenosis point, potentially influencing the blood flow velocity pattern in the LCA.

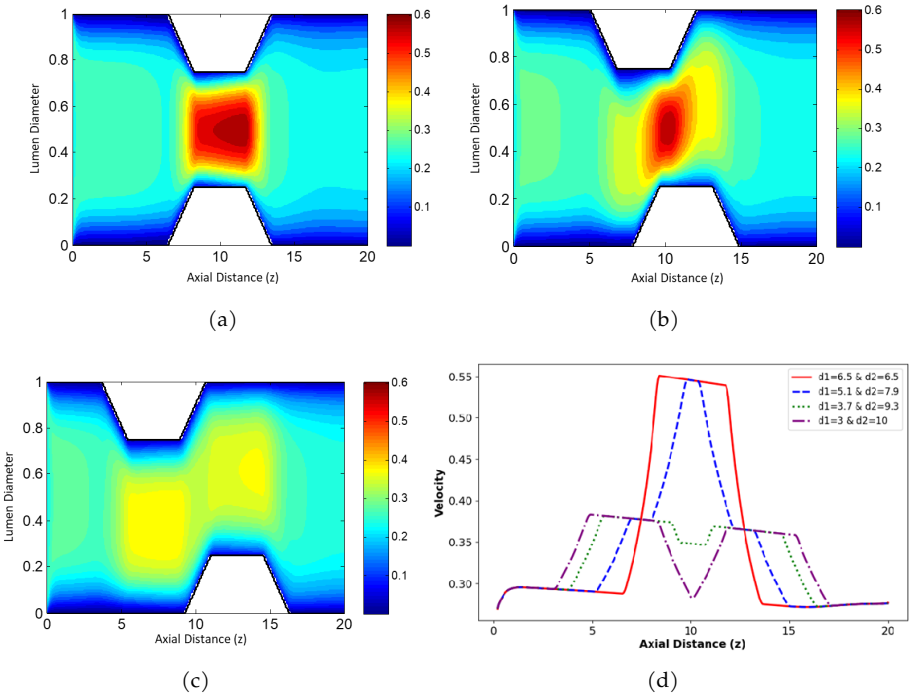

Figure 13: Flow velocity contours for different stenosis locations within a symmetric Trapezoidal geometry.

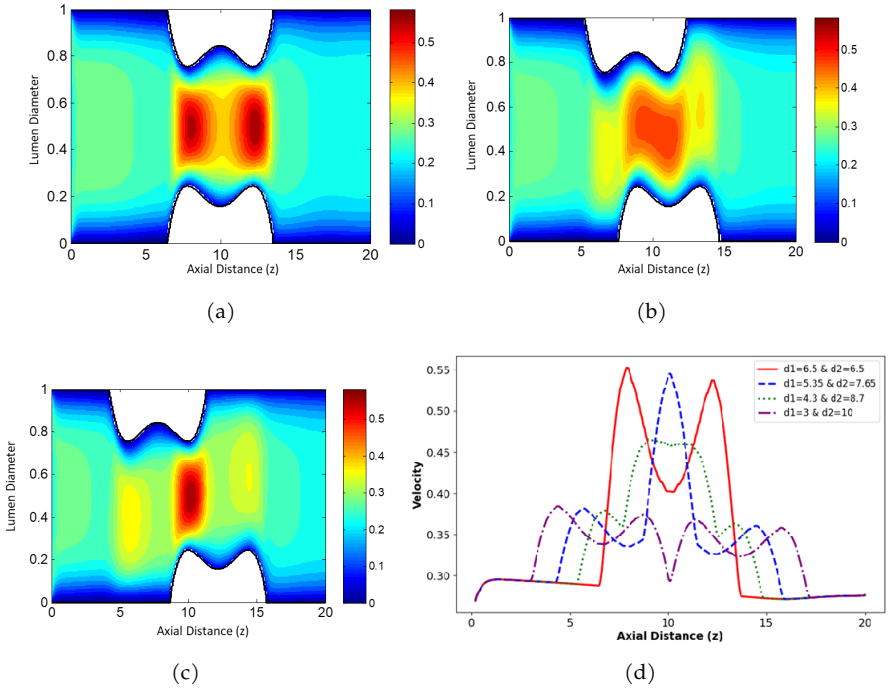

Figure 14: Flow velocity contours for different stenosis locations within a symmetric Overlapping (W-shape) geometry.

The results indicate that the stenosis location significantly affects the distribution of blood flow velocity in the LCA. If the stenosis occurs closer to the inlet, the high-velocity zone is reached faster. Conversely, when the stenosis shifts to the middle section, the peak velocity and acceleration area move along with the stenosis location. This change can increase the risk of further plaque formation. Thus, the severity of flow disturbance is determined not only by the degree of stenosis but also by of disturbed flow, but also the stenosis position along the vessel.

In Figure 14(a), the flow accelerates around the stenosis area, resulting in a more visible red zone (indicating high velocity) in that region. After passing the constricted part, the flow velocity begins to decrease, shown by yellow colors. Figures 14(a), 14(b) and 14(c), show a more pronounced velocity increase in the shifted stenosis area according to its position. Within the stenosis zone, flow tends to have relatively lower velocity. Overall, the farther the stenosis position shifts, the longer the area where the fluid prepares before acceleration at the stenosis point, which potentially influences the blood flow velocity pattern in the LCA.

The effect of stenosis severity on pressure distribution is illustrated in Figure 15. At a 25% narrowing (Figure 15(a)), the pressure drop is minimal and confined to the stenotic throat (yellow area). This pressure decrease becomes more significant at 50% stenosis (Figure 15(b)), as shown by the transition to green. Finally, the 75% stenosis case (Figure 15(c)) exhibits the most substantial pressure drop of 11418.2 Pa, visualized as a blue area at the center of the constriction.

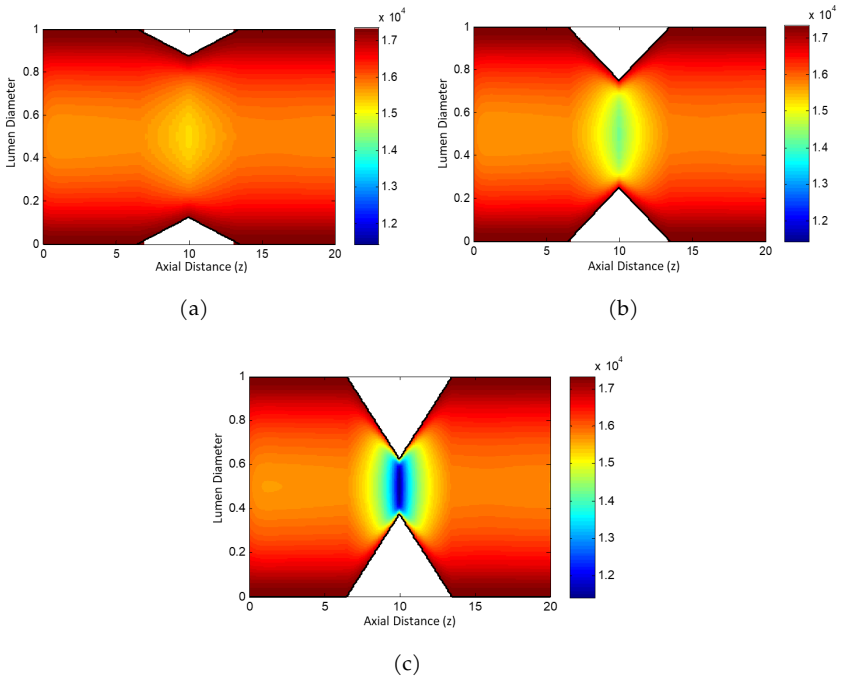

Figure 15: Pressure distribution contours under varying stenosis severities in a symmetric Triangular geometry: (a) 25% stenosis, (b) 50% stenosis, (c) 75% stenosis.

In Figure 16, the pressure distribution at 25% stenosis in Figure 16(a) shows a pattern resembling trapezoidal stenosis. At 50% stenosis in Figure 16(b), the yellow-green zone in the stenosis area indicates an increasingly evident pressure drop, signaling a larger pressure decrease around the stenosis. As shown in Figure 16(c), when the stenosis reaches 75%, the blue region representing low pressure (11353.73 Pa) expands significantly at the center of the constriction, exhibiting a pattern similar to that observed in the triangular stenosis model. This indicates a pronounced drop in pressure within the narrowed segment.

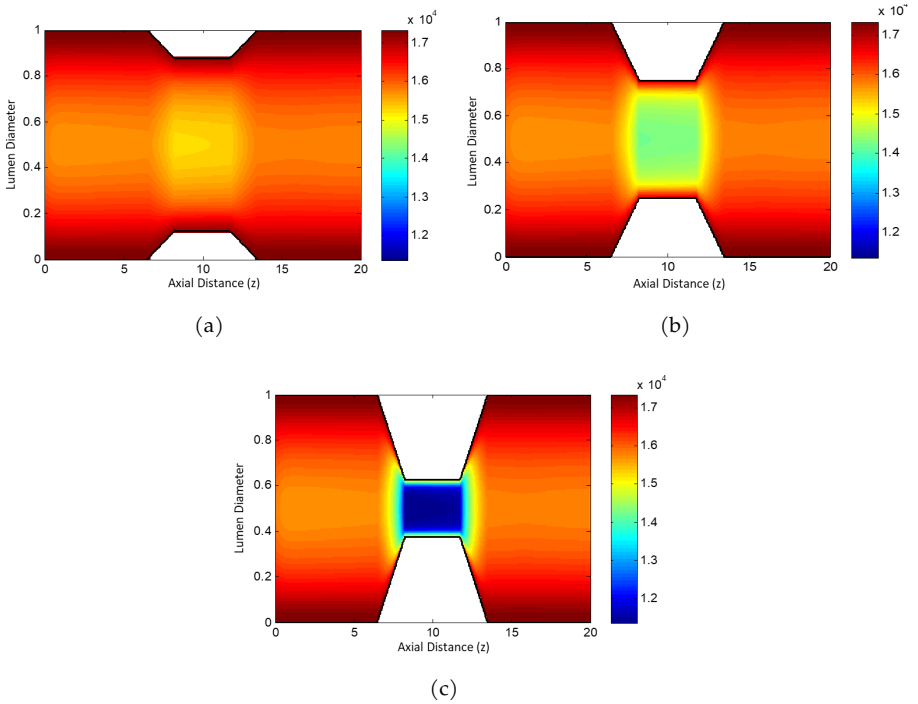

Figure 16: Pressure distribution contours under varying stenosis severities in a symmetric Trapezoidal geometry: (a) 25% stenosis, (b) 50% stenosis, (c) 75% stenosis.

Figure 17 confirms that a higher degree of stenosis significantly influences the pressure distribution along the channel. At 25% stenosis in Figure 17(a), the pressure drop is still relatively small, shown by the dominance of orange-yellow colors around the stenosis area. When stenosis increases to 50% in Figure 17(b), the low-pressure zone becomes more apparent, with the emergence of green color near the stenosis center. Meanwhile, at 75% stenosis, the blue area expands and spreads around the stenosis center, indicating a significant pressure drop of 11683.28 Pa due to the increased degree of stenosis.

Figure 18 shows the effect of stenosis position on flow pressure distribution in triangular stenosis. In Figure 18(a), the stenosis is centered symmetrically, resulting in a low-pressure area marked by dark blue around the stenosis peak. In Figure 18(b), the low-pressure zone is more dominant in the middle of the stenosis, with a more uniform pressure drop. Lastly, in Figure 18(c), the stenosis position is further downstream, causing the high-pressure distribution to be more uniform across the area.

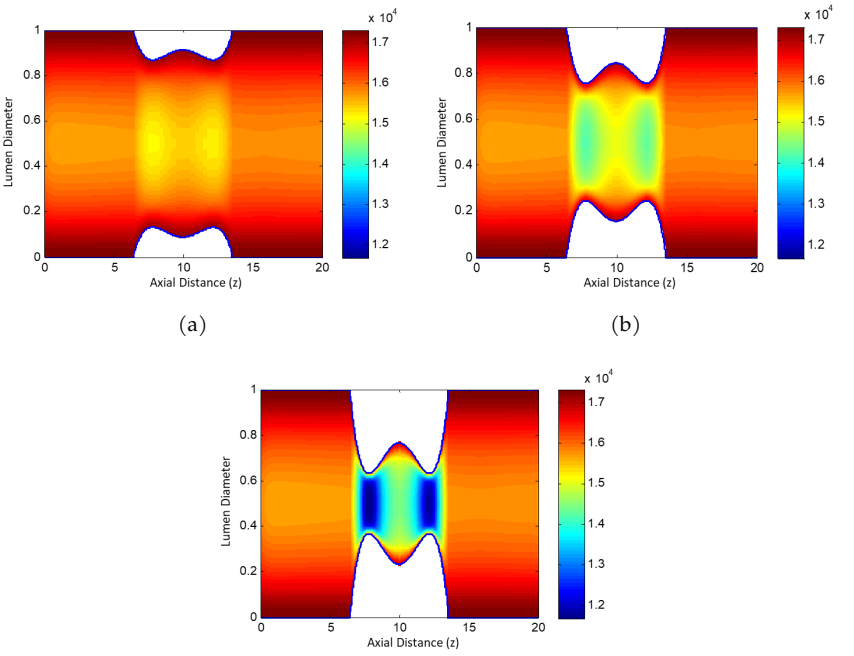

Figure 17: Pressure distribution contours under varying stenosis severities in a symmetric Overlapping (W-shape) geometry: (a) 25% stenosis, (b) 50% stenosis, (c) 75% stenosis.

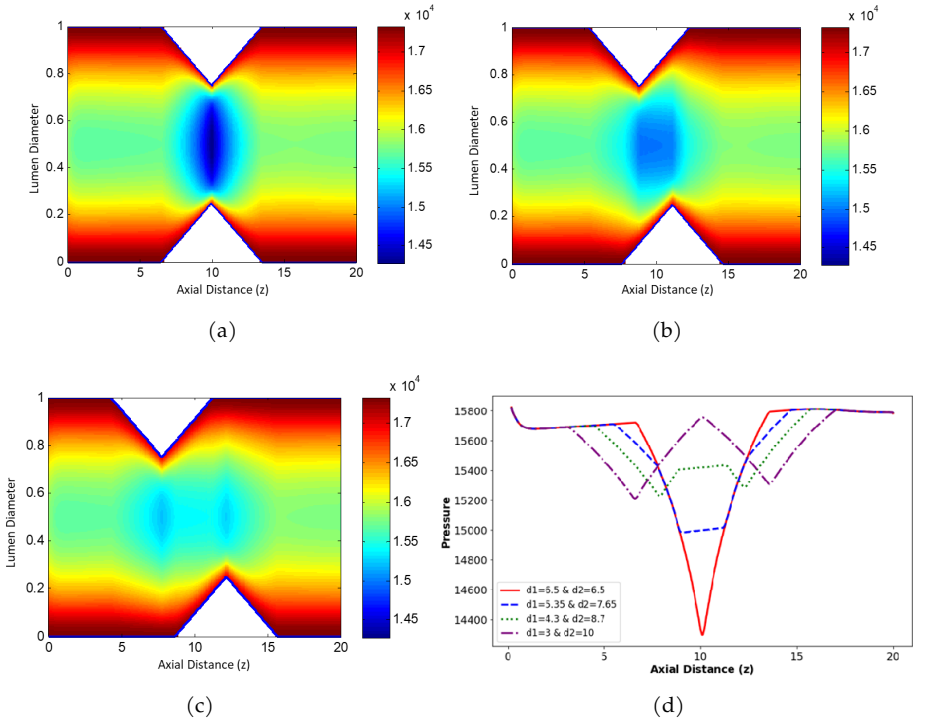

Figure 18: Pressure distribution contours for different stenosis positions in a symmetric Triangular shaped geometry.

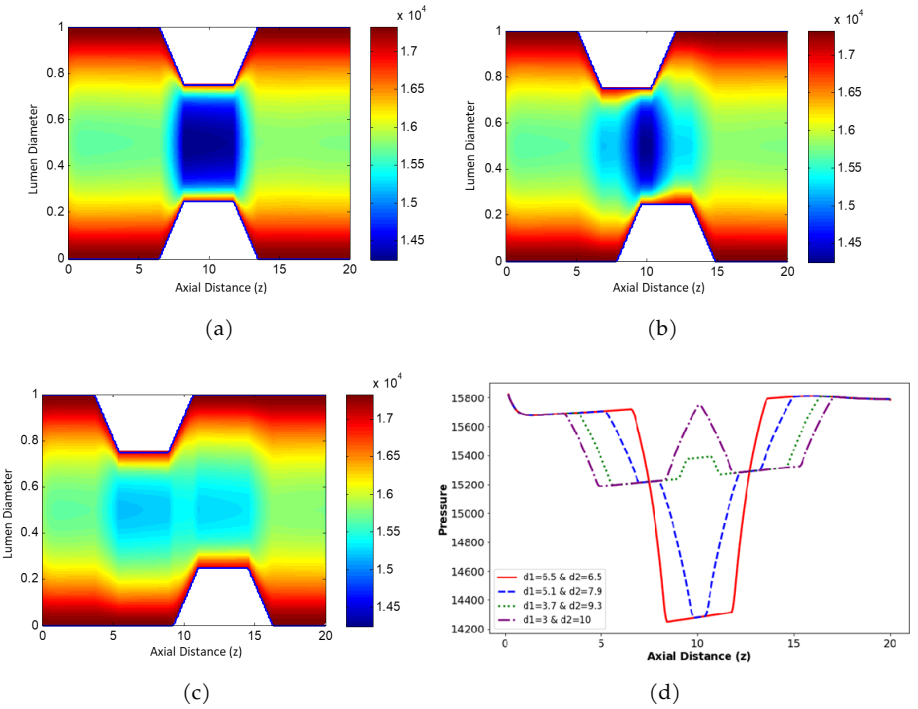

Figure 19: Pressure distribution contours for different stenosis positions in a symmetric Trapezoidal shaped geometry.

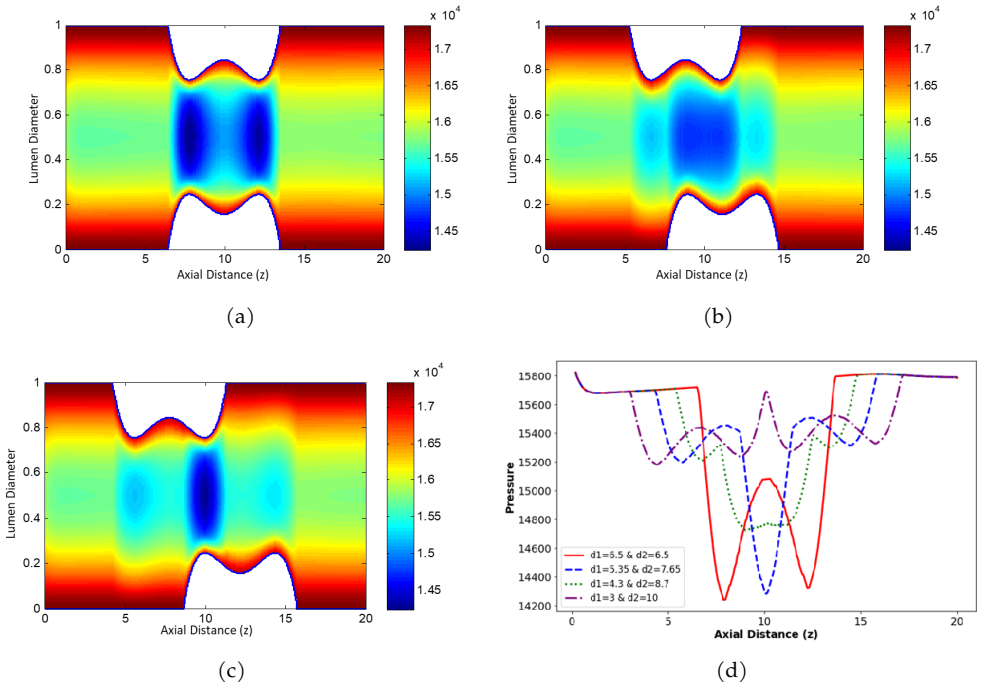

Figure 20: Pressure distribution contours for different stenosis positions in a symmetric Overlapping (W-shape) geometry.

Figure 19 illustrates the effect of varying stenosis position on flow pressure distribution in trapezoidal shape. In Figure 19(a), the stenosis is located at the center, forming a dark blue low-pressure zone at the peak. In contrast, in Figure 19(b), the low-pressure region shifts to the middle of the stenosis, with a more uniform pressure drop pattern compared to before. Meanwhile, in Figure 19(c), the farthest stenosis position shift results in consistently high pressure because the pressure distribution from stenosis is more balanced.

Figure 20 shows the impact of stenosis position on flow pressure distribution in W-shape stenosis. In Figure 20(a), the centrally located stenosis causes low pressure at the peak, marked by dark blue. Subsequently, in Figure 20(b), the low-pressure zone is more concentrated in the middle of the stenosis, with a relatively small pressure drop and a more balanced distribution. Figure 20(c) shows pressure contours with no significant changes, where blue color still dominates most of the area. Finally, in Figure 20(d), the stenosis at the farthest position maintains high pressure because the stenosis effect is more optimally distributed.

Based on Figures 21−23, the trapezoidal model shows the highest wall shear stress compared to the other models, especially at 75% stenosis, reaching 42.7 Pa. Physically, wall shear stress (WSS) represents the tangential frictional force exerted by the flowing blood on the arterial wall surface. The high WSS values, particularly in the trapezoidal model at 75% stenosis, are caused by the very steep velocity gradients near the arterial wall. The sharp acceleration of the flow along the flat 'peak' of the trapezoidal stenosis maximizes this gradient. From a biological standpoint, abnormally high WSS is known to cause direct injury to endothelial cells, trigger an inflammatory response, and increase the risk of plaque rupture, a primary trigger for myocardial infarction. While wall shear stress is relatively moderate at 25% to 50% stenosis levels, the abrupt escalation observed at 75% suggests a heightened potential for vascular injury. Excessive shear forces of this magnitude may trigger platelet activation, promote localized thrombosis, and eventually lead to vessel occlusion, This indicates that a trapezoidal-shaped stenosis is particularly conducive to the advancement of LCA disease. Additionally, the sudden shift from moderate to severe WSS indicates that individuals with the same stenotic pattern may face sudden hemodynamic instability, highlighting the need for early medical intervention to prevent total arterial occlusion.

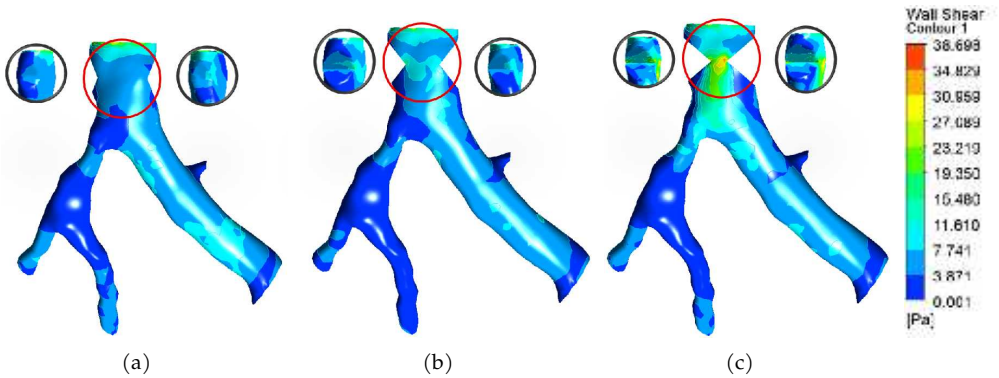

Figure 21: Wall shear stress plots on the coronary vessel surface for the Triangular model: (a) 25% stenosis, (b) 50% stenosis, (c) 75% stenosis.

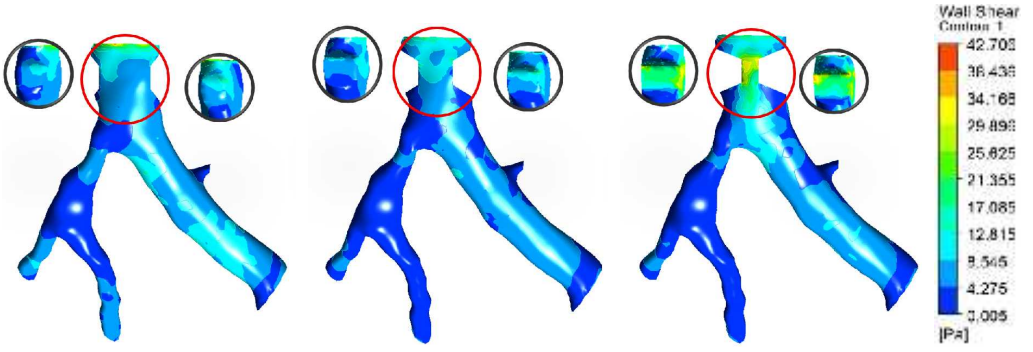

Figure 22: Wall shear stress plots on the coronary vessel surface for the Trapezoidal model: (a) 25% stenosis, (b) 50% stenosis, (c) 75% stenosis.

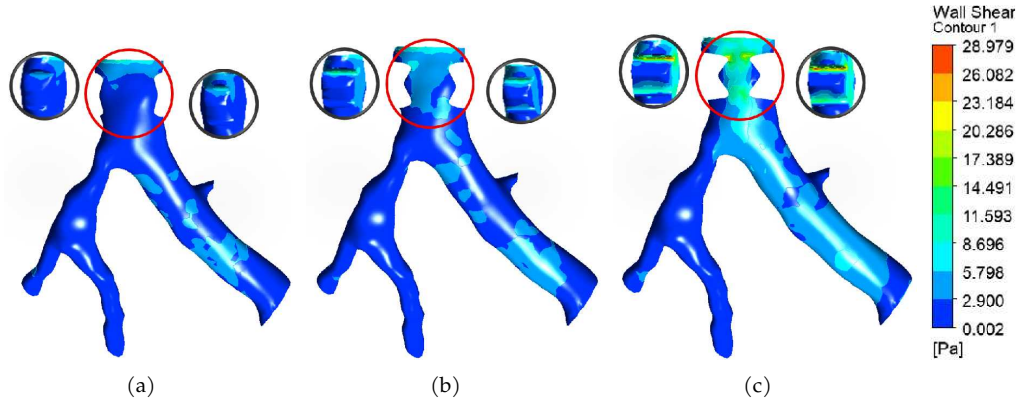

Figure 23: Wall shear stress plots on the coronary vessel surface for the Overlapping (W-shape) model: (a) 25% stenosis, (b) 50% stenosis, (c) 75% stenosis.

This study has several limitations inherent to computational modeling. We assumed a rigid, impermeable arterial wall, and future work should incorporate vascular elasticity through Fluid-Structure Interaction (FSI) and the effects of wall porosity for greater physiological accuracy [27, 26]. Similarly, while the idealized geometries used here provide a crucial baseline, further investigations are needed to explore other geometrical configurations such as bell-shaped, cosine, and elliptical profiles, as well as asymmetrical constriction conditions where the upper and lower stenosis profiles differ. The next step is to integrate patient-specific models from medical imaging to capture the complexity of real lesions. Ultimately, such advanced models will allow for a more comprehensive investigation into the interplay between patient-specific geometry and other physiological factors, such as the biomagnetic response of blood.

4 Conclusion

This study aims to numerically analyze the impact of blood flow constriction in the LCA as a cause of cardiovascular disease, using the Finite Volume Method. Coronary artery narrowing, especially due to plaque buildup, can disrupt blood flow, potentially increasing the risk of coronary

artery disease (CAD), heart attacks, and strokes. Through simulations conducted with various constriction shapes-Triangular, Trapezoidal, and Overlapping (W-shape)-at different stenosis levels, this study provides insights into the effects of narrowing on blood flow velocity, pressure distribution, and shear stress in the vessels. Based on the simulation results, the following conclusions can be drawn:

- When the arterial narrowing reaches 50%, the blood flow velocity starts to show abnormal values around 0.5 m/s, with a noticeable increase that signals disruption in the flow. At 75% narrowing, the velocity sharply rises to over 1 m/s, indicating a shift toward disturbed flow that can lead to turbulence and higher shear stress on the vessel walls. This increase in velocity can worsen the condition of the blood vessels, raising the risk of damage, plaque buildup, and potentially heart attacks or strokes. Narrowing beyond 50% requires serious medical attention to prevent further complications. Moreover, the trapezoidal shaped narrowing poses a higher risk with flow velocity recorded at 1.06755 m/s compared to other shapes of constriction.
- Constrictions with increasingly shifted positions tend to reduce blood flow velocity due to more distributed flow patterns. This suggests that more varied stenosis poses a lower risk compared to symmetric constriction.
- All constriction shapes at 75% stenosis cause significant pressure drops. The trapezoidal shape is associated with the largest pressure drop (to $11,353.73$ Pa), creating a steep pressure gradient indicative of high flow acceleration and stress, which has the potential to damage blood vessels.
- The trapezoidal model generates the highest wall shear stress, especially at 75% stenosis, reaching 42.7 Pa. This indicates a higher potential for vascular damage and thrombosis.
- Sharp shifts in Wall Shear Stress (WSS) at severe stenosis indicate hemodynamic instability, underscoring the need for early medical intervention to prevent serious complications such as total arterial occlusion.
- Future work will involve the integration of real stenosis geometries derived from patient specific anatomical data obtained through MRI imaging.

Acknowledgement The authors gratefully acknowledge the full support of the Laboratory of Modelling and Mathematics Computation (Mathcom), Department of Mathematics Education, University of Jember, Indonesia, as well as the Center for Research on Computational Mathematics (CERCOM), Faculty of Applied Sciences and Technology, Universiti Tun Hussein Onn Malaysia.

Conflicts of Interest The authors declare that we have no conflicts of interest to reveal.

References

[1] M. G. Al-Azawy, S. K. Kadhim & A. S. Hameed (2020). Newtonian and non-Newtonian blood rheology inside a model of stenosis. *CFD Letters*, *12*(11), 27–36. https://doi.org/10.37934/cfdl.12.11.2736.

[2] A. Athani, N. N. N. Ghazali, I. A. Badruddin, A. Y. Usmani, S. Kamangar, A. E. Anqi & N. A. Ahammad (2021). Two-phase non-Newtonian pulsatile blood flow simulations in a rigid

and flexible patient-specific left coronary artery (LCA) exhibiting multi-stenosis. *Applied Sciences*, *11*(23), Article ID: 11361. https://doi.org/10.3390/app112311361.

[3] P. Boutouyrie, P. Chowienczyk, J. D. Humphrey & G. F. Mitchell (2021). Arterial stiffness and cardiovascular risk in hypertension. *Circulation Research*, *128*(7), 864–886. https://doi.org/10.1161/CIRCRESAHA.121.318061.

[4] W. Deng & K.-i. Tsubota (2022). Numerical simulation of the vascular structure dependence of blood flow in the kidney. *Medical Engineering & Physics*, *104*, Article ID: 103809. https://doi.org/10.1016/j.medengphy.2022.103809.

[5] B. M. Egan (2018). Defining hypertension by blood pressure 130/80 mm Hg leads to an impressive burden of hypertension in young and middle-aged black adults: Follow-up in the CARDIA study. *Journal of the American Heart Association*, *7*(14), Article ID: e009971. https://doi.org/10.1161/JAHA.118.009971.

[6] J. P. Empana, F. Canoui Poitrine, G. Luc, I. Juhan Vague, P. Morange, D. Arveiler, J. Ferrieres, P. Amouyel, A. Bingham, M. Montaye, J. B. Ruidavets, B. Haas, A. Evans & P. Ducimetiere (2008). Contribution of novel biomarkers to incident stable angina and acute coronary syndrome: The PRIME study. *European Heart Journal*, *29*(16), 1966–1974. https://doi.org/10.1093/eurheartj/ehn331.

[7] A. Fatahillah, B. Widodo & R. Roslan (2025). The modeling and numerical solution of branch retinal artery occlusion. *Malaysian Journal of Mathematical Sciences*, *19*(1), 1–16. https://doi.org/10.47836/mjms.19.1.01.

[8] A. Fatahillah, B. Widodo & R. Roslan (2025). Mathematical modeling and numerical simulation of central retinal artery occlusion (CRAO) with asymmetric stenosis. *Statistics, Optimization and Information Computing*, *13*(5), 2079–2104. https://doi.org/10.19139/soic-2310-5070-2381.

[9] J. H. Ferziger & M. Perić (2002). *Computational Methods for Fluid Dynamics*. Springer, Berlin, Germany. https://doi.org/10.1007/978-3-642-56026-2.

[10] P. Goswami, D. Mandal, N. Manna & S. Chakrabarti (2014). Study on the effect of steady, simple pulsatile and physiological pulsatile flows through a stenosed artery. *Heat and Mass Transfer*, *50*(10), 1343–1352. https://doi.org/10.1007/s00231-014-1334-0.

[11] M. Kaewbumrung, S. Orankitjaroen, P. Boonkrong, B. Nuntadilok & B. Wiwatanapataphee (2018). Numerical simulation of dispersed particle-blood flow in the stenosed coronary arteries. *International Journal of Differential Equations*, *2018*(1), Article ID: 2593425. https://doi.org/10.1155/2018/2593425.

[12] A. Karimipour, D. Toghraie, L. A. Abdulkareem, A. Alizadeh, M. Zarringhalam & A. Karimipour (2020). Roll of stenosis severity, artery radius and blood fluid behavior on the flow velocity in the arteries: Application in biomedical engineering. *Medical Hypotheses*, *144*, Article ID: 109864. https://doi.org/10.1016/j.mehy.2020.109864.

[13] S. Kumar & T. K. R. Rajagopal (2021). Effect of reynold's number on effective heat transfer dissipation of braking system. *Materials Today: Proceedings*, *46*(Part 17), 8455–8460. https://doi.org/10.1016/j.matpr.2021.03.488.

[14] D. Lopes, R. Agujetas, H. Puga, J. Teixeira, R. Lima, J. P. Alejo & C. Ferrera (2021). Analysis of finite element and finite volume methods for fluid-structure interaction simulation of blood flow in a real stenosed artery. *International Journal of Mechanical Sciences*, *207*, Article ID: 106650. https://doi.org/10.1016/j.ijmecsci.2021.106650.

[15] A. K. Malakar, D. Choudhury, B. Halder, P. Paul, A. Uddin & S. Chakraborty (2019). A review on coronary artery disease, its risk factors, and therapeutics. *Journal of Cellular Physiology*, *234*(10), 16812–16823. https://doi.org/10.1002/jcp.28350.

[16] M. M. Martins, M. Vaz Jr & P. S. B. Zdanski (2018). A note on a derivative scheme for the finite volume method applied to incompressible viscous fluid. *Continuum Mechanics and Thermodynamics*, *30*(4), 943–952. https://doi.org/10.1007/s00161-018-0649-3.

[17] T. Morofuji, M. Saito, S. Inaba, H. Morioka & T. Sumimoto (2018). Prognostic value of proximal left coronary artery flow velocity detected by transthoracic Doppler echocardiography. *IJC Heart & Vasculature*, *19*, 52–57. https://doi.org/10.1016/j.ijcha.2018.04.003.

[18] A. M. Morrison, A. E. Sullivan & A. W. Aday (2023). Atherosclerotic disease: Pathogenesis and approaches to management. *Medical Clinics of North America*, *107*(5), 793–805. https://doi.org/10.1016/j.mcna.2023.04.004.

[19] T. Mukha, R. E. Bensow & M. Liefvendahl (2021). Predictive accuracy of wall-modelled large-eddy simulation on unstructured grids. *Computers & Fluids*, *221*, Article ID: 104885. https://doi.org/10.1016/j.compfluid.2021.104885.

[20] S. Nadeem, S. Akhtar, A. Saleem, N. Akkurt, H. A. Ghazwani & S. M. Eldin (2023). Numerical computations of blood flow through stenosed arteries via CFD tool OpenFOAM. *Alexandria Engineering Journal*, *69*, 613–637. https://doi.org/10.1016/j.aej.2023.02.005.

[21] R. Pandey, M. Kumar & V. K. Srivastav (2020). Numerical computation of blood hemodynamic through constricted human left coronary artery: Pulsatile simulations. *Computer Methods and Programs in Biomedicine*, *197*, Article ID: 105661. https://doi.org/10.1016/j.cmpb.2020.105661.

[22] H. Parthasarathy, O. Saeed, D. Marcuzzi & A. N. Cheema (2013). MRI-induced stent dislodgment soon after left main coronary artery stenting. *Circulation: Cardiovascular Interventions*, *6*(5), e58–e59. https://doi.org/10.1161/CIRCINTERVENTIONS.112.000790.

[23] M. F. Rabbi, F. S. Laboni & M. T. Arafat (2020). Computational analysis of the coronary artery hemodynamics with different anatomical variations. *Informatics in Medicine Unlocked*, *19*, Article ID: 100314. https://doi.org/10.1016/j.imu.2020.100314.

[24] R. G. Rajagopalan & A. D. Lestari (2016). RK-SIMPLER: Explicit time-accurate algorithm for incompressible flows. *AIAA Journal*, *54*(2), 616–624. https://doi.org/10.2514/1.J054030.

[25] M. Roy, B. S. Sikarwar, M. Bhandwal & P. Ranjan (2017). Modelling of blood flow in stenosed arteries. *Procedia Computer Science*, *115*, 821–830. https://doi.org/10.1016/j.procs.2017.09.164.

[26] B. D. Sharma & P. K. Yadav (2017). A two-layer mathematical model of blood flow in porous constricted blood vessels. *Transport in Porous Media*, *120*, 239–254. https://doi.org/10.1007/s11242-017-0918-9.

[27] B. D. Sharma & P. K. Yadav (2018). A mathematical model of blood flow in narrow blood vessels in presence of magnetic field. *National Academy of Sciences Letters*, *42*, 239–243. https://doi.org/10.1007/s40009-018-0718-y.

[28] D. Sukmawati (2023). Peran penting inflamasom NLRP3 pada aterosklerosis. *Jurnal Penyakit Dalam Indonesia*, *10*(2), Article ID: 8. https://doi.org/10.7454/jpdi.v10i2.1417.

[29] K. M. M. Than & M. W. Khin (2019). Teaching effects of numeric integration by using MATLAB programming. *International Journal for Advance Research and Development*, *4*(8), 16–20. https://www.ijarnd.com/manuscripts/v4i8/V4I8-1143.pdf.

[30] M. N. Uddin, M. M. Uddin & M. M. Alam (2022). Comparative mathematical study of blood flow through stenotic and aneurysmatic artery with the presence and absence of blood clots. *Malaysian Journal of Mathematical Sciences*, *16*(3), 599–623. https://doi.org/10.47836/mjms.16.3.12.

[31] H. K. Versteeg & W. Malalasekera (2007). *An Introduction to Computational Fluid Dynamics: The Finite Volume Method*. Pearson Education Limited, Essex, England.

[32] K. K. Wong, J. Wu, G. Liu, W. Huang & D. N. Ghista (2020). Coronary arteries hemodynamics: Effect of arterial geometry on hemodynamic parameters causing atherosclerosis. *Medical & Biological Engineering & Computing*, *58*(8), 1831–1843. https://doi.org/10.1007/s11517-020-02185-x.

[33] B. Xie & F. Xiao (2016). A multi-moment constrained finite volume method on arbitrary unstructured grids for incompressible flows. *Journal of Computational Physics*, *327*, 747–778. https://doi.org/10.1016/j.jcp.2016.09.054.

[34] P. K. Yadav & A. Singh (2025). Biomedical simulations of electroosmotic non-Newtonian hybrid nanofluid (blood) with hematocrit viscosity through a porous overlapping irregular stenosed artery. *Computers in Biology and Medicine*, *196*(Part B), Article ID: 110575. https://doi.org/10.1016/j.compbiomed.2025.110575.

[35] N. M. Zain & Z. Ismail (2023). Numerical solution of magnetohydrodynamics effects on a generalised power law fluid model of blood flow through a bifurcated artery with an overlapping shaped stenosis. *PLoS ONE*, *18*(2), Article ID: e0276576. https://doi.org/10.1371/journal.pone.0276576.